Journal of Science and Technology – Smart Systems and Devices
Volume x, Issue x, Month Year, ppp-ppp

Frequency-Constrained Unit Commitment Using Offline Frequency-Response Screening

Huy Nguyen Duc**, Cuong Hoang Anh, Anh Phung Van, Alexander Vo
School of Electrical and Electronic Engineering, Hanoi University of Science and Technology, Ha Noi, Vietnam
**Corresponding author email: huy.nguyenduc1@hust.edu.vn*

Abstract
This paper presents a frequency-constrained unit commitment (FCUC) framework in which post-contingency rate-of-change-of-frequency (RoCoF) and frequency-nadir criteria are translated into generator-commitment constraints. For each system, offline screening of commitment states using a center-of-inertia (COI)-based average system frequency response (ASFR) model identifies minimum requirements for equivalent inertia, a turbine-response index, and inverse droop. These requirements are imposed as linear constraints, preserving the mixed-integer linear programming (MILP) formulation. The framework is evaluated on the IEEE 39-bus and WECC-179 systems. For WECC-179, Ward-based Q–V zoning and area-level reactive-power balance constraints are also included as a surrogate for reactive-power adequacy. COI/ASFR post-checks show that the FCUC schedules satisfy the design-contingency criteria within the screening model. For IEEE 39, under a 0.60 Hz/s RoCoF limit, FCUC commits all 10 units, compared with 7–9 under conventional UC, with a 2.79% increase in scheduling cost. For WECC-179, scheduling raises the UC-to-FCUC objective from 14.323 to 14.929 million USD (+4.229%). Independent ANDES time-domain simulations for the loss of G2 show that FCUC reduces the worst-case RoCoF from 0.64 to 0.49 Hz/s and raises the minimum nadir from 59.78 to 59.79 Hz. Taken together, these results demonstrate that interpretable aggregate frequency-response requirements can be embedded in UC while retaining its MILP structure and explicitly revealing the trade-off between scheduling cost and post-contingency frequency security.

Keywords: Average system frequency response, center of inertia, frequency nadir, frequency-constrained unit commitment, rate of change of frequency.

1. Introduction

The objective of conventional unit commitment (UC) is to minimize the operating cost subject to energy, unit, and reserve constraints. Regarding dynamic system response, static reserve constraints do not ensure an acceptable frequency trajectory after large disturbances. As inverter-based generation displaces synchronous machines, a low-cost schedule may provide too little inertia or primary response to arrest the frequency decline following generation loss events. To overcome this drawback, frequency-constrained UC (FCUC) links commitment decisions to these post-contingency metrics. Its central challenge is to relate system responses to the decision variables in UC without making scheduling intractable.

The fundamental approach to solving the FCUC problem is to derive UC-compatible limits from center-of-inertia (COI), and to formulate an average system frequency response (ASFR) model [1]. The approach can be further fine-tuned in different aspects. In [2], the authors simulated a complete set of hourly operating conditions in PSS/E with N-1 contingencies, and established a linear regression of the frequency nadir. [3] proposes a linear-exponential-decay frequency curve that compactly represents pre-nadir dynamics and drives unit-specific frequency-nadir-response calculations, taking into account each resource's reserve headroom and internal saturation. [4] resolves the post-contingency response trajectory in concrete delivery times and activation delays, while [5] shows that fast response units help reduce the commitment cost related to security constraints. The effect of locational frequency is studied in [6], where it is shown that system-wide inertia and the total primary frequency response can be insufficient. The locational RoCoF limits derived from network modes are also included in security-constrained UC [7]. Other studies address the stochastic nature of frequency response. A two-stage robust formulation preserves dispatch non-anticipativity under sequential uncertainty [8], while Bayesian filtering yields a posterior distribution of frequency trajectories that supports a chance-constrained nadir requirement [9].

UC-compatible formulations include two-stage nadir linearization [10], continuous-time links [11], offline labelled-state rules [12], and physics-guided piecewise-linear surrogates [13]. Resource-rich variants co-optimize fast BESS injection under wind uncertainty [14] or wind-turbine regulation and primary-frequency reserves [15]. In contrast, this study retains conventional generator response and emphasizes transparent offline

p-ISSN 3093-3285
e-ISSN 3093-3315
https://doi.org/10.51316/jst.xxx.saad.xxxx.xx.x.x
Received: Sep 3, 2026; Revised: Sep 30, 2026;
Accepted: Oct 3, 2026; Online: Nov 16, 2026

In press

screening and independent cross-model validation. These formulations have system- and objective-dependent trade-offs [16].

We follow Wu *et al.* [1] in generating the screening data offline with the COI/ASFR model. Because COI/ASFR represents the system by one equivalent frequency, it addresses the system-wide dynamics; locational dynamics remain outside the scope of this study. The workflow evaluates commitment combinations using RoCoF and nadir, converts the secure set into UC-compatible limits, and then post-checks the resulting schedules. The specific contributions are threefold. First, a cross-scale implementation maps secure states into linear limits on equivalent inertia, turbine-response index, and inverse droop. Second, the IEEE 39 schedules are independently checked in ANDES [17] using an inertia-weighted COI, enabling a transparent comparison between screening and dynamic simulation. Third, frequency-security cuts are combined with Ward Q–V zones in WECC-179 scheduling.

2. Model and Computational Procedure

2.1. Conventional UC

For generating unit i at time t, the main decision variables are power output $P_{i,t}$, commitment status $u_{i,t} \in \{0,1\}$, startup variable $y_{i,t}$, and shutdown variable $z_{i,t}$. The objective function is

$$\min \sum_t \sum_i \left(c_i P_{i,t} + c_i^{\mathrm{NL}} u_{i,t} + c_i^{\mathrm{SU}} y_{i,t} + c_i^{\mathrm{SD}} z_{i,t} \right) \quad (1)$$

Here, c_i, c_i^{NL}, c_i^{SU}, and c_i^{SD} are the energy, no-load, startup, and shutdown costs; D_t and R_t denote hourly demand and reserve. The basic constraints include

$$\sum_i P_{i,t} = D_t \quad (2)$$

$$P_i^{\min} u_{i,t} \le P_{i,t} \le P_i^{\max} u_{i,t} \quad (3)$$

$$\sum_i (P_i^{\max} u_{i,t} - P_{i,t}) \ge R_t \quad (4)$$

together with ramping, minimum up/down-time, startup–shutdown logic, and initial-status constraints. The frequency constraints do not replace spinning reserve; instead, they are added as a separate security layer.

2.2. COI/ASFR and Equivalent Parameters

In a multi-machine system, the frequencies of synchronous generators are not identical after a disturbance because of relative rotor oscillations. COI frequency is an inertia-weighted average that describes the bulk motion of the system and provides a representative system frequency rather than separate frequencies for individual rotors. On this basis, the ASFR model reduces the multi-machine system to a low-order equivalent that aggregates inertia, frequency-dependent load sensitivity, droop, and turbine–governor response; the model structure is shown in Fig. 1.

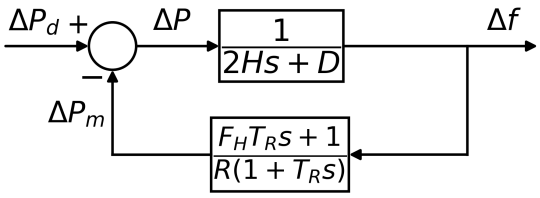


Fig. 1. Average system frequency response model, adapted from [1]

With $P_\Sigma = \sum_i P_i^{\max}$ and $K_i = P_i^{\max}/P_\Sigma$, the COI frequency at time t is given by

$$f_{\mathrm{COI},t}^{(k)} = \frac{\sum_{i \ne k} u_{i,t} K_i H_i f_{i,t}}{\sum_{i \ne k} u_{i,t} K_i H_i} \quad (5)$$

For the design contingency involving the trip of unit k, the remaining units are aggregated on the same system base:

$$H_{s,t}^{(k)} = \sum_{i \ne k} u_{i,t} K_i H_i \quad (6)$$

$$R_{s,t}^{-1(k)} = \sum_{i \ne k} u_{i,t} \frac{K_i}{R_i} \quad (7)$$

Define $S_{R,t}^{(k)} = R_{s,t}^{-1(k)}$. The equivalent governor parameters used in the ASFR post-check are

$$F_{H,t}^{(k)} = \frac{\sum_{i \ne k} u_{i,t} F_{H,i} K_i / R_i}{S_{R,t}^{(k)}} \quad (8)$$

$$T_{R,t}^{(k)} = \frac{\sum_{i \ne k} u_{i,t} T_{R,i} K_i / R_i}{S_{R,t}^{(k)}} \quad (9)$$

The power imbalance is normalized by the total $P_i^{\max}$:

$$P_{\mathrm{loss,pu}} = \frac{P_{\mathrm{loss}}}{\sum_i P_i^{\max}} \quad (10)$$

and the initial RoCoF is evaluated as

$$\mathrm{RoCoF}_t = \frac{P_{\mathrm{loss,pu}} f_0}{2 H_{s,t}^{(k)}} \quad (11)$$

During screening, P_{loss} is set equal to the rated power $P_k^{\max}$ of the tripped unit. In the hourly post-check, P_{loss} is taken as the output of this unit immediately before the contingency. Let $R_t^{(k)} = 1/R_{s,t}^{-1(k)}$ and $A_t = 1 + D R_t^{(k)}$, and omit the indices t, k for compactness. The characteristic parameters of the second-order response are

$$\omega_n = \sqrt{\frac{A}{2 H_s R T_R}}, \quad (12)$$

$$\zeta = \frac{\omega_n [2 H_s R + (DR + F_H) T_R]}{2A} \quad (13)$$

$$\omega_r = \omega_n \sqrt{1 - \zeta^2} \quad \Delta f_{\mathrm{ss}} = f_0 \frac{P_{\mathrm{loss,pu}} R}{A} \quad (14)$$

In press

For $\zeta < 1$, the time to nadir and the frequency deviation at the nadir are calculated as

$$t_{\mathrm{n}} = \frac{1}{\omega_r}\,\mathrm{atan2}(\omega_r T_R, \zeta\omega_n T_R - 1) \tag{15}$$

$$\alpha = \sqrt{\frac{1 - 2T_R\zeta\omega_n + (T_R\omega_n)^2}{1-\zeta^2}} \tag{16}$$

$$\Delta f_{\mathrm{n}} = \Delta f_{\mathrm{ss}}\left[1 + \sqrt{1-\zeta^2}\,\alpha e^{-\zeta\omega_n t_{\mathrm{n}}}\right] \tag{17}$$

$$f_{\mathrm{nadir}} = f_0 - \Delta f_{\mathrm{n}}, \quad f_{\mathrm{final}} = f_0 - \Delta f_{\mathrm{ss}} \tag{18}$$

For $\zeta \geq 1$, the response has no transient oscillation, and the nadir deviation is set to $\Delta f_{\mathrm{n}} = \Delta f_{\mathrm{ss}}$. The nadir expressions are nonlinear in the commitment combination and are therefore used only for screening and post-check evaluation; the FCUC problem uses linear bounds derived from the set of secure states.

2.3. Screening and FCUC Constraints

A commitment combination is considered secure only when it satisfies both

$$\mathrm{RoCoF} \leq \mathrm{RoCoF}_{\max}, \qquad f_{\mathrm{nadir}} \geq f_{\min} \tag{19}$$

Let $g_i = K_i/R_i$ and use the fixed post-contingency denominator $S_R^{\mathrm{base},(k)} = \sum_{j\neq k} g_j$. For $i \neq k$,

$$h_i = K_i H_i, \qquad r_i = g_i, \qquad q_i = \frac{F_{H,i} g_i}{S_R^{\mathrm{base},(k)}} \tag{20}$$

whereas $h_k = q_k = r_k = 0$ for the tripped unit. The FH_{lin} index uses a fixed denominator and differs from the ratio $F_{H,t}^{(k)}$ in (8), which is used only for screening and ASFR post-checks. Here, H_{lim} follows analytically from (11), while FH_{lim} and R_{lim}^{-1} are component-wise minima of the secure states; the resulting classifier is validated against all screened states. The FCUC cuts are

$$\sum_i h_i u_{i,t} \geq H_{\mathrm{lim}} \tag{21}$$

$$\sum_i q_i u_{i,t} \geq FH_{\mathrm{lim}} \tag{22}$$

$$\sum_i r_i u_{i,t} \geq R_{\mathrm{lim}}^{-1} \tag{23}$$

The coefficients of the unit tripped in the design contingency are set to zero. Because all three constraints are linear in $u_{i,t}$, the FCUC problem retains its MILP structure and can be solved using commercial solvers. The overall procedure consists of five steps: generate valid commitment combinations of the remaining units; evaluate the RoCoF and nadir of each combination using the COI/ASFR model; classify secure combinations and determine the three bounds H_{lim}, FH_{lim}, and R_{lim}^{-1}; solve FCUC with the frequency constraints; and post-check the optimal schedule, with the IEEE 39 schedule additionally subjected to dynamic validation in ANDES.

Throughout the study, only one design contingency is considered for each system when constructing the FCUC constraints: the complete loss of G2 (646 MW) in IEEE 39 and the loss of G6 (5393.53 MW) in WECC-179. The remaining scenarios—a +1000 MW load step in IEEE 39, and the loss of G8 and G18 in WECC-179—are used only as supplementary post-checks and are not used to construct the constraints. WECC-179 is not subjected to ANDES dynamic validation within the scope of this paper.

2.4. Q–V Zoning and Reactive-Power Constraints

Frequency is a system-wide quantity, so one set of COI-based constraints can represent the whole network response. Voltage on the other hand, need to be controlled locally. In a compact network, treating the system as a single zone is adequate. However, in a large system with long transmission corridors, such as WECC-179, reactive power balance should be accounted for. We address this by augmenting the FCUC formulation with analysis of voltage control area. Following the electrical-distance approach of Lagonotte *et al.* [18], small changes of reactive power and voltage around the operating point are related by

$$\Delta Q = J_{QV}\Delta V \tag{24}$$

$$S_{VQ} = J_{QV}^{-1} \tag{25}$$

$$d_{ij} = -\log\left(\frac{|S_{VQ,ij}|}{\sqrt{|S_{VQ,ii}S_{VQ,jj}|}}\right) \tag{26}$$

Here J_{QV} is the Jacobian block relating reactive-power variations to voltage, and S_{VQ} gives how far the voltage at bus i moves when reactive power is injected at bus j. Equation (26) turns that influence into a distance: buses that strongly affect each other receive a small d_{ij}, buses that barely interact receive a large one. Ward clustering then merges the closest buses into voltage-control areas.

Within each area z, the schedule must keep the reactive output of every unit inside its own limits, retain a margin for raising and for lowering voltage, and balance local reactive supply against local demand and the exchange with neighbouring areas:

$$Q_g^{\min} \leq q_{g,t} \leq Q_g^{\max}, \qquad g \in \mathscr{G}_z \tag{27}$$

$$\sum_{g\in\mathscr{G}_z}\left(Q_g^{\max}u_{g,t} - q_{g,t}\right) \geq Q_{z,t}^{up} \tag{28}$$

$$\sum_{g\in\mathscr{G}_z}\left(q_{g,t} - Q_g^{\min}u_{g,t}\right) \geq Q_{z,t}^{down} \tag{29}$$

$$\sum_{g\in\mathscr{G}_z} q_{g,t} - \sum_{z'} q_{zz',t}^{tie} = Q_{z,t}^{dem} \tag{30}$$

Here $q_{g,t}$ is the representative reactive-power variable of a generating unit; $Q_{z,t}^{up}$ and $Q_{z,t}^{down}$ are the upward and downward Q-reserve requirements of area z; and $q_{zz',t}^{tie}$ is the reactive-power exchange between areas. The constraints are linear in $q_{g,t}$ and $u_{g,t}$, so they preserve the MILP structure of Section 2.3.

In press

3. IEEE 39-Bus Case Study

3.1. System Data and FCUC Parameters

The IEEE 39 system has 39 buses, 46 branches, and 10 generating units. The UC set has an aggregate $P_{\max}$ of 7367 MW; the 24-hour load ranges from 4065.2 to 6254.2 MW and peaks at hour 19. The main case excludes wind and BESS, requires 5% spinning reserve, and keeps G10 online as the slack unit.

3.2. Screening for the Loss of G2

Screening and ANDES use the same rating base and inertia-weighted COI, with the tripped G2 omitted. Offline screening replaces non-binding 0.85 Hz/s with 0.60 Hz/s, excluding low-inertia states while retaining a secure set. The thresholds are

$$H_{\text{lim}} = 2.9528, \qquad FH_{\text{lim}} = 0.4762, \qquad R_{\text{lim}}^{-1} = 18.4715. \tag{31}$$

with $f_0 = 60$ Hz, $f_{\min} = 59.5$ Hz and $\text{RoCoF}_{\max} = 0.60$ Hz/s. All 256 states (G10 fixed online; G2 zeroed post-trip) are screened exhaustively. The only secure pre-contingency state commits all 10 units; hence, the FH_{lim} and R_{lim}^{-1} cuts enforce all units, while H_{lim} is slack.

The effect of equivalent inertia on the frequency response is shown in Fig. 2. As H_s increases, the frequency nadir tends to improve because the initial rate of frequency decline is limited.

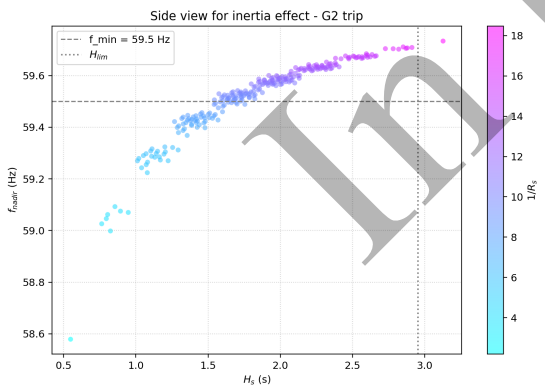


Fig. 2. Effect of equivalent inertia H_s on the frequency nadir following the loss of G2

In addition to inertia, turbine-response characteristics affect the frequency nadir. The relationship between the F_H index and the frequency nadir is presented in Fig. 3.

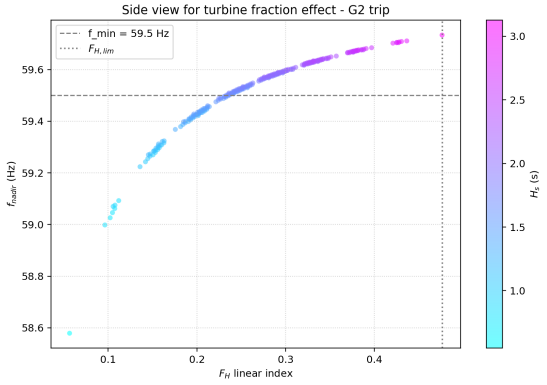


Fig. 3. Effect of the turbine-response index F_H on the frequency nadir following the loss of G2

The primary frequency response capability of online units is represented by the aggregate inverse droop. Fig. 4 shows that the frequency nadir generally increases as this index increases.

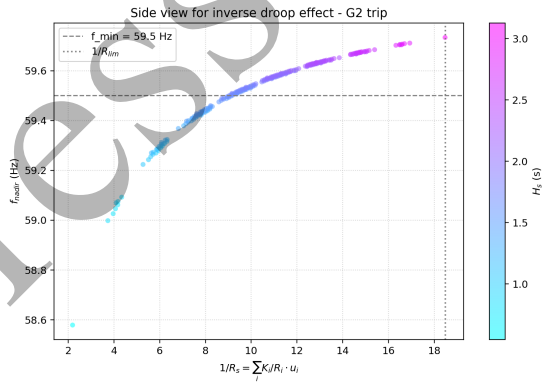


Fig. 4. Effect of inverse droop on the frequency nadir following the loss of G2

The commitment combinations are then classified as secure or insecure according to the joint RoCoF and frequency-nadir criteria. Fig. 5 illustrates the secure and insecure regions in the linear-index space used to determine the bounds incorporated into FCUC.

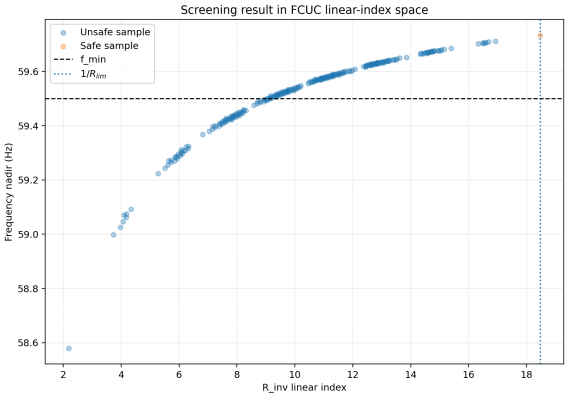


Fig. 5. Classification of secure and insecure regions in the linear-index space

In press

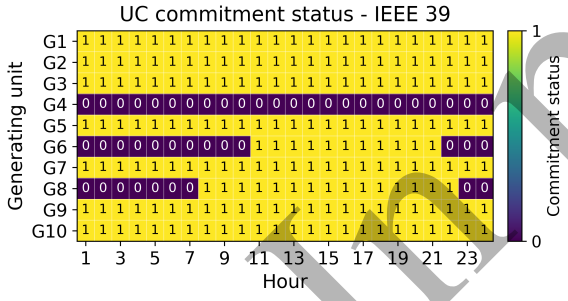
3.3. UC/FCUC Schedules and Cost

Conventional UC requires only 7–9 units online; G4 remains offline throughout the 24-hour horizon, while G6 and G8 are committed as the load increases. In contrast, the three frequency constraints require FCUC to keep all 10 units online. Table 1 summarizes the corresponding economic and commitment metrics. Fig. 6 compares the commitment status, while Fig. 7 presents the generation mix of the two schedules.

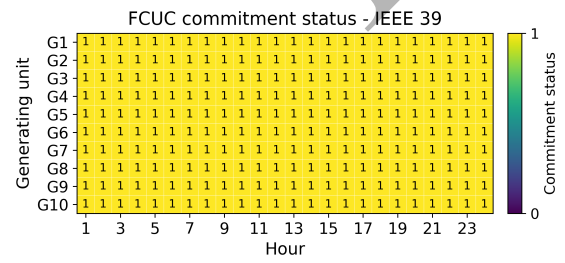
Table 1. Economic and commitment comparison for IEEE 39

Metric	**UC**	**FCUC**
Total cost	2,681,625	2,756,554
Difference	–	+74,929 (2.79%)
Minimum reserve	6.543%	17.792%
Minimum online units	7	10
Maximum online units	9	10
G10 online	24/24	24/24

The cost increase should not be interpreted simply as "purchasing additional reserve." FCUC changes which units are online, thereby increasing both inertia and governor response capability. This is consistent with the observation in [2, 4] that inertia alone does not fully represent the capability to maintain the frequency nadir.

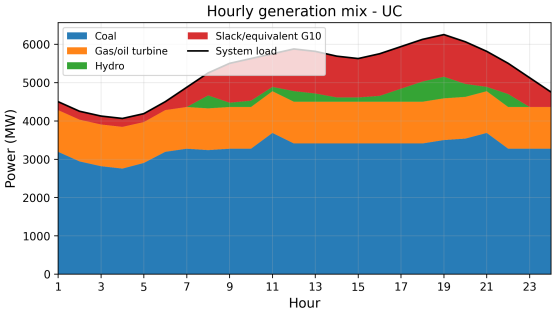


(a) UC: online/offline status.

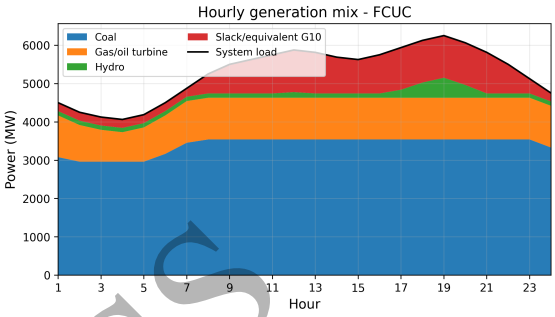


(b) FCUC: online/offline status.

Fig. 6. Comparison of UC and FCUC commitment status in IEEE 39 over 24 hours



(a) UC: generation mix.



(b) FCUC: generation mix.

Fig. 7. Comparison of the UC and FCUC generation mixes in IEEE 39 over 24 hours

3.4. COI/ASFR Post-Checks: G2 and a 1000 MW Load Step

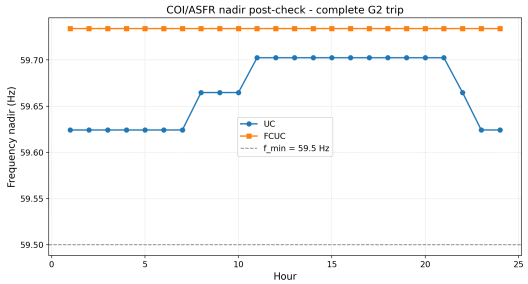
For G2, UC produces three representative commitment groups based on the number of online units. The results in Table 2 show that UC fails to satisfy the combined criterion over the 24-hour horizon because of RoCoF. Although the UC nadir satisfies the limit in all 24 hours, RoCoF remains above 0.60 Hz/s in every hour. In contrast, FCUC satisfies both the RoCoF and nadir limits in all 24 hours.

Table 2. COI/ASFR post-check groups for the G2 contingency.

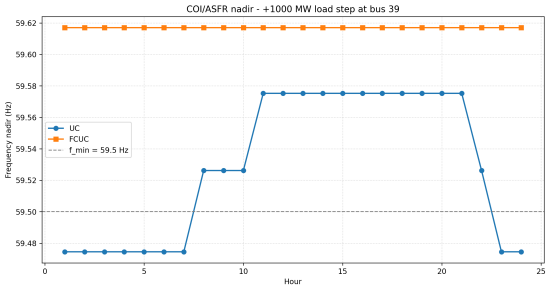
Hour	**ON**	H_s	R^{-1}	**RoCoF Hz/s**	**Nadir Hz**
1–7,23–24	7	2.2588	12.5647	0.7843	59.6242
8–10,22	8	2.4743	14.3386	0.7160	59.6647
11–21	9	2.8197	16.3236	0.6283	59.7024
FCUC 1–24	10	3.1269	18.4715	0.5666	59.7338

Fig. 8 presents the 24-hour post-check results for the loss of G2 and the +1000 MW load step. The load step is an out-of-design scenario and is therefore not used to construct the FCUC constraints. In this scenario, neither UC nor FCUC simultaneously satisfies both COI/ASFR criteria. Nevertheless, FCUC raises the minimum nadir from 59.47 to 59.62 Hz and reduces the maximum RoCoF from 1.10 to 0.82 Hz/s.

In press



(a) COI/ASFR nadir following the loss of G2.



(b) COI/ASFR nadir for a 1000 MW load increase.

Fig. 8. 24-hour COI/ASFR post-checks for IEEE 39

4. Dynamic Validation of IEEE 39 Using ANDES

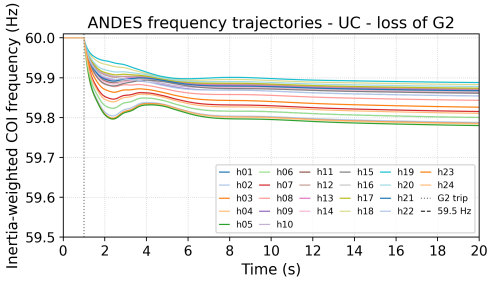
4.1. Validation Configuration

COI/ASFR is an equivalent model used for optimization and rapid post-check evaluation; ANDES provides a more detailed, independent validation layer. A separate dynamic case is constructed for each hour, and the power flow must converge before the time-domain simulation (TDS). TDS runs from 0 to 20 s, the event occurs at $t = 1$ s, and the simulation time step is 0.01 s. For G2, the unit remains in its pre-contingency state and is tripped by an event during TDS. RoCoF is extracted as the maximum-magnitude finite difference within a 0.5 s post-contingency window. The ANDES scenario is the loss of G2.

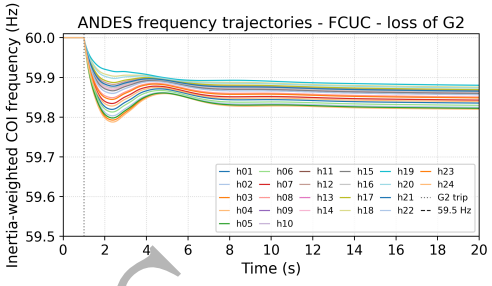
4.2. Primary Contingency: Loss of G2

The 24-hour ANDES simulation results for the loss of G2 differ substantially from the COI/ASFR post-checks: both UC and FCUC maintain the nadir above the 59.5 Hz threshold. Fig. 9(a)–(b) presents the frequency trajectories of the two schedules, while Fig. 9(c) compares the hourly nadirs.

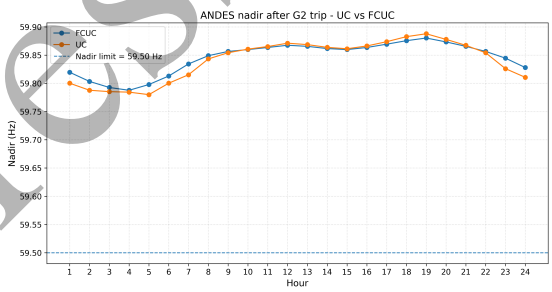
The minimum nadir over the horizon is 59.78 Hz for UC and 59.79 Hz for FCUC; the corresponding maximum RoCoF values are 0.64 and 0.49 Hz/s. These results indicate that the COI/ASFR model is more conservative for this case. FCUC improves the worst-case values over the horizon, but this should not be interpreted as FCUC always outperforming UC at every operating state.



(a) UC: 24 frequency trajectories.



(b) FCUC: 24 frequency trajectories.



(c) Hourly nadir over 24 hours.

Fig. 9. ANDES simulation results for the loss of G2

5. WECC-179 Extension

5.1. Configuration and G6 Screening Results

The screening procedure described in Section 2.3 is applied to WECC-179, which comprises 179 buses, 29 generating units, and 122,416 MW of installed capacity. The model uses lossless DC-UC and a 12-area Ward Q–V representation; spinning reserve is 10%, G17 remains online, and the design contingency is the loss of G6 with $P_{\text{loss}} = 5393.53$ MW. The evaluation criteria are $f_{\min} = 59.5$ Hz and $\text{RoCoF}_{\max} = 0.50$ Hz/s.

The zoning procedure of Section 2.4 was applied to WECC-179 around the base operating point, and twelve voltage-control areas were retained. The areas contain 17, 12, 32, 6, 16, 24, 8, 22, 13, 3, 14, and 12 buses and are linked by 29 inter-area reactive-power exchanges; G8 and G9 fall in area 4, while G22 falls in area 8. Fig. 10 shows the partition on the network. The area constraints (27)–(30) were enforced on these twelve areas in the UC and FCUC runs of Section 5.2, whose objectives are therefore reported for the Q–V-constrained model.

In press

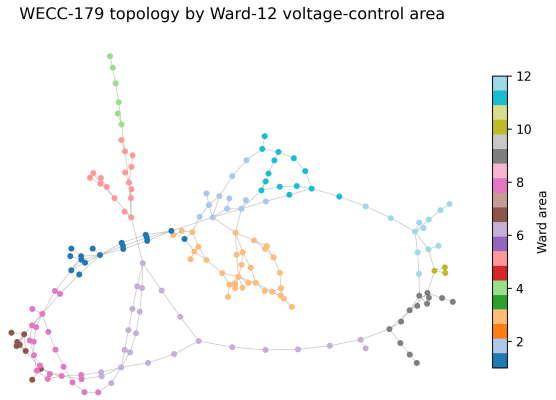


Fig. 10. WECC-179 topology with 12 voltage-control areas determined using Ward clustering

The screening results yield the following limits:

$$H_{\text{lim}} = 2.6435, \qquad FH_{\text{lim}} = 0.2047$$
$$R_{\text{lim}}^{-1} = 14.7552 \tag{32}$$

With G17 fixed online and G6 zeroed post-trip, $2^{27} = 134{,}217{,}728$ states remain. We evaluate 1,000,000 uniformly generated Bernoulli samples (seed 20260623); 10,872 satisfy both frequency criteria. Fig. 11 summarizes the screening results for the G6 design contingency.

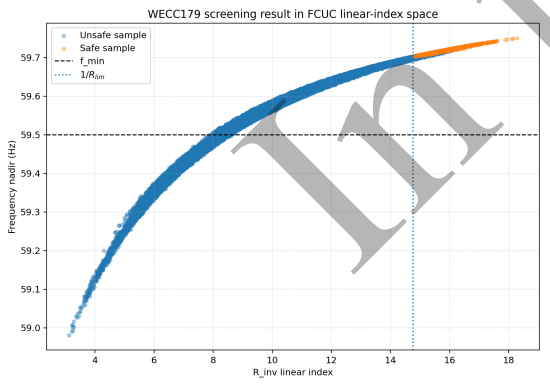
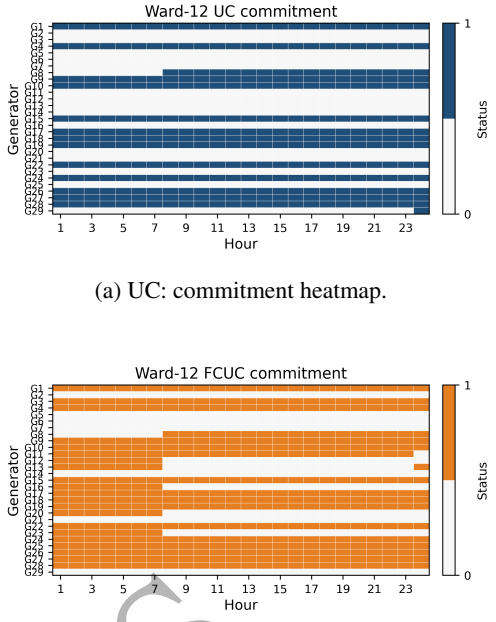


Fig. 11. WECC-179 screening results for the G6 design contingency: classification of secure states

5.2. UC/FCUC and G8/G18 Post-Checks

Simulation results showed that UC commits 13–15 units and FCUC 17–21; the objective rises from 14.323 to 14.929 million USD (+4.229%). Fig. 12 and Fig. 13 show the schedules and the G18 nadir post-check.



(a) UC: commitment heatmap.

(b) FCUC: commitment heatmap.

Fig. 12. WECC-179 UC and FCUC commitment heatmaps.

The G8/G18 post-checks show that the response is contingency-dependent. For G8, both UC and FCUC satisfy the combined criteria in all 24 hours; the minimum nadir increases from 59.808 to 59.823 Hz, and the maximum RoCoF decreases from 0.356 to 0.323 Hz/s. For G18, the nadirs of both schedules remain above 59.5 Hz, but RoCoF exceeds 0.5 Hz/s in several hours; UC satisfies the criteria in 9 of the 24 hours and FCUC in 16 of the 24 hours. Because G8/G18 are only out-of-design post-checks relative to G6, the results do not provide a multi-contingency guarantee and motivate the robust and scenario-based FCUC approaches in [8, 9, 13].

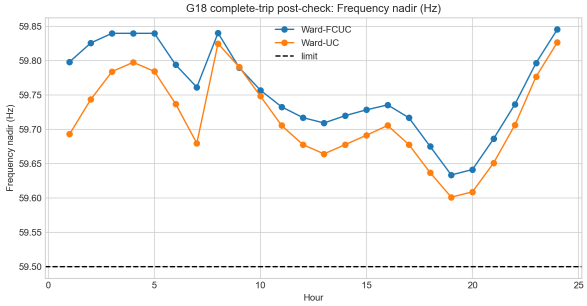


Fig. 13. Nadir post-check following the loss of G18

6. Conclusions and Future Work

This study has developed a consistent FCUC procedure comprising baseline UC, offline screening using the COI/ASFR model, conversion of secure regions into linear constraints, solution of the unit commitment problem, and post-check evaluation. Results for both systems demonstrate that nonlinear frequency criteria

In press

can be transformed into a transparent set of linear constraints compatible with the MILP structure; however, the resulting security benefits must be evaluated together with the cost of additional commitment.

The current model still has some limitations. First, COI/ASFR is a low-order equivalent model and tends to be conservative compared with dynamic simulation; it does not fully capture locational differences, detailed governor characteristics, inter-machine oscillations, or the effects of different operating conditions. Second, the FCUC constraints for each system are constructed from a single design contingency and therefore do not guarantee multi-contingency security.

Future work should also develop multi-contingency FCUC using robust or stochastic approaches while accounting for uncertainty in load, renewable generation, and contingency magnitude. In addition, the inertia, primary-response, and nadir constraints should be calibrated using detailed dynamic simulations or data-driven surrogates to reduce the conservatism of the screening stage. These extensions would enable the simultaneous assessment of network feasibility, frequency security, and operating cost within a practically applicable unit commitment framework.

Reference

[1] J.-J. Wu, G. W. Chang, C. Sinatra, and P.-Y. Tsai, Unit commitment with frequency stability enhancement for an isolated power system, IEEE access : practical innovations, open solutions, vol. 12, pp. 91396–91409, Jul. 2024. https://doi.org/10.1109/ACCESS.2024.3421628

[2] X. Liu, X. Fang, N. Gao, H. Yuan, A. Hoke, H. Wu, and J. Tan, Frequency nadir constrained unit commitment for high renewable penetration island power systems, IEEE Open Access Journal of Power and Energy, vol. 11, pp. 141–153, Feb. 2024. https://doi.org/10.1109/OAJPE.2024.3370504

[3] G. Yan, L. Yan, Y. Meng, J. Han, and Z. Li, Linear-exponential decay frequency curve for unit-specific response in frequency-constrained unit commitment, IEEE Transactions on Power Systems, vol. 41, iss. 5, pp. 3548–3565, Sep. 2026. https://doi.org/10.1109/TPWRS.2026.3685128

[4] L. Badesa, F. Teng, and G. Strbac, Optimal portfolio of distinct frequency response services in low-inertia systems, IEEE Transactions on Power Systems, vol. 35, iss. 6, pp. 4459–4469, Nov. 2020. https://doi.org/10.1109/TPWRS.2020.2997194

[5] R. Shikuma, Y. Fujimoto, D. Orihara, H. Kikusato, H. Taoka, and Y. Hayashi, Impact of virtual synchronous generators on frequency-constrained unit commitment: a neural network-assisted framework for assessing rate of change of frequency, IEEE access : practical innovations, open solutions, vol. 13, pp. 117716–117731, Jul. 2025. https://doi.org/10.1109/ACCESS.2025.3585194

[6] L. Badesa, F. Teng, and G. Strbac, Conditions for regional frequency stability in power system scheduling—Part II: Application to Unit Commitment, IEEE Transactions on Power Systems, vol. 36, iss. 6, pp. 5567–5577, Nov. 2021. https://doi.org/10.1109/TPWRS.2021.3073077

[7] M. Tuo and X. Li, Security-constrained unit commitment considering locational frequency stability in low-inertia power grids, IEEE Transactions on Power Systems, vol. 38, iss. 5, pp. 4134–4147, Sep. 2023. https://doi.org/10.1109/TPWRS.2022.3215915

[8] S. Zhao, Z. Wei, Y. Fang, X. Liu, and S. Sun, Frequency constrained unit commitment under multi-uncertainty: a robust and non-anticipative implicit decision method, CSEE Journal of Power and Energy Systems, 2026. https://doi.org/10.17775/CSEEJPES.2024.06570

[9] Y. Yuan, Y. Cao, Z. Zhang, W. Hu, and Z. Chen, Refined frequency-constrained unit commitment under converter-induced uncertain-variability through bayesian filtering, IEEE Transactions on Power Systems, vol. 41, iss. 5, pp. 3302–3322, Sep. 2026. https://doi.org/10.1109/TPWRS.2026.3684036

[10] Q. Shi, Y. Zhu, K. Fan, R. Cheng, J. Shen, and W. Liu, Two-stage linearization of frequency nadir constraint for unit commitment, IEEE Transactions on Power Systems, vol. 40, iss. 4, pp. 3584–3587, Jul. 2025. https://doi.org/10.1109/TPWRS.2025.3564110

[11] M. Rajabdorri, E. Lobato, L. Sigrist, and J. Aghaei, Data-driven continuous-time framework for frequency-constrained unit commitment, International Journal of Electrical Power & Energy Systems, vol. 162, Nov. 2024, Art. no. 110327. https://doi.org/10.1016/j.ijepes.2024.110327

[12] A. O. Olasoji, D. T. O. Oyedokun, M. Rajabdorri, J. E. Sierra-Aguillar, C. E. Okafor, M. Mditshwa, and K. A. Folly, Frequency-Constrained Unit Commitment Using SODE-labelled Affine Surrogates, in 2026 8th Global Power, Energy and Communication Conference (GPECOM), pp. 703–708, Jun. 2026.

[13] S. H. Beigi Fard, M. R. Shakarami, and M. Doostizadeh, Frequency-constrained robust unit commitment via physics-guided piecewise-linear nadir surrogates and adaptive virtual inertia, Scientific Reports, vol. 16, Mar. 2026, Art. no. 14305. https://doi.org/10.1038/s41598-026-43137-z

[14] Y. Wen, W. Li, G. Huang, and X. Liu, Frequency Dynamics constrained unit commitment with battery energy storage, IEEE Transactions on Power Systems, vol. 31, iss. 6, pp. 5115–5125, Nov. 2016. https://doi.org/10.1109/TPWRS.2016.2521882

[15] B. Jiang, C. Guo, and Z. Chen, Frequency constrained unit commitment considering reserve provision of wind power, Applied Energy, vol. 361, May 2024, Art. no. 122898. https://doi.org/10.1016/j.apenergy.2024.122898

[16] M. Sarvarizadeh, M. Rajabdorri, E. Lobato, and L. Sigrist, A Comparative Study on Frequency-Constrained Unit Commitment Approaches in Island Power Systems, arXiv preprint arXiv:2507.05079, Jul. 2025.

[17] H. Cui, F. Li, and K. Tomsovic, Hybrid symbolic-numeric framework for power system modeling and analysis, IEEE Transactions on Power Systems, vol. 36, iss. 2, pp. 1373–1384, Mar. 2021. https://doi.org/10.1109/TPWRS.2020.3017019

[18] J. Y. Leost and J. P. Paul, Structural Analysis of the Electrical System: Application to Secondary Voltage Control in France, IEEE Transactions on Power Systems, vol. 4, iss. 2, pp. 479–486, May 1989. https://doi.org/10.1109/59.193819

In press